Electron-paramagnetic-resonance investigation of the iron-indium pair in silicon

W. Gehlhoff,* P. Emanuelsson, P. Omling, and H. G. Grimmeiss
Department of Solid State Physics, University of Lund, Box 118, S-221 00 Lund, Sweden
(Received 26 October 1992)

A defect consisting of a substitutional indium and an interstitial iron ion in silicon has been studied using the electron-paramagnetic-resonance (EPR) technique. The defect is found to appear in two different configurations, where the iron ion occupies two different interstitial positions near the substitutional indium ion. In the first case the symmetry is trigonal and in the second case orthorhombic. For the orthorhombic configuration, two EPR spectra were detected and they were found to originate in transitions within the two Kramers doublets of a spin-$\frac{3}{2}$ system with a large zero-field splitting. These two spectra show a very complicated hyperfine structure, which could be successfully explained by taking the hyperfine, nuclear Zeeman, and quadrupole interactions into account. Based on the result of the analysis, we suggest that both the trigonal and the orthorhombic spectra originate in the $^4T_1$ state of the ^4F ground state of Fe^+ ($3d^7$), split by a cubic crystal field.

I. INTRODUCTION

Pairs made up of a transition metal and a group-III acceptor in silicon have been extensively studied in recent years. In particular, the physics of the pairs between iron and shallow acceptors has stimulated a great deal of research ever since the pioneering electron-paramagnetic-resonance (EPR) work of Ludwig and Woodbury.[1] They studied the iron-boron, iron-gallium, and iron-indium pairs and determined that the microscopic structure has trigonal symmetry for FeB and FeGa and orthorhombic symmetry for the FeIn pair. They suggested that these defects consist of an acceptor on a substitutional site and an iron atom on the nearest (FeB and FeGa) or next-nearest (FeIn) interstitial site. Later, van Kooten, Weller, and Ammerlaan found two different FeAl pairs, one with trigonal and one with orthorhombic symmetry,[2] and recently Gehlhoff, Irmscher, and Kreissl studied the FeGa defect in the orthorhombic configuration.[3] They also detected new EPR spectra for the orthorhombic FeAl and FeGa pairs. To explain the existence of two orthorhombic EPR line sets, they proposed a model in which the spin is $\frac{3}{2}$ and the zero-field splitting is large. It is suggested that the EPR transitions take place within the two Kramers doublets of the $S=\frac{3}{2}$ system. The energy levels of these defects have been determined using space-charge techniques.[4,5]

Interest in iron-acceptor pairs increased considerably in 1985 when Chantre and Bois in their deep-level-transient-spectroscopy (DLTS) measurements observed a metastable behavior of the FeAl pair, i.e., they showed that the defect could switch between trigonal (nearest-neighbor, or possibly fourth-nearest-neighbor) and orthorhombic (next-nearest-neighbor) configuration.[6] Later it was shown that the FeGa and FeIn pairs also possess metastable properties.[7] From the DLTS measurements it was quite clear that each configuration gives rise to a deep donor in the band gap. By combining EPR and DLTS measurements, Gehlhoff, Irmscher, and Rehse demonstrated the correspondence between the two different configurations and the two hole traps for FeAl.[8]

In spite of these efforts, there are still open questions about iron-acceptor pairs which need to be solved. The DLTS measurements have revealed two different configurations for the FeIn pair, while only one of them, the orthorhombic, is detected by EPR. For FeAl and FeGa there are two different EPR spectra for the orthorhombic configuration, while for FeIn only one is reported. Furthermore, if we interpret the FeIn spectrum in the same way as in the case of FeAl and FeGa ($S=\frac{3}{2}$, large zero-field splitting) and assume that the observed resonance is the one within the lower doublet, then we get the opposite sign for the axial fine-structure parameter compared with FeAl and FeGa. These problems were recently solved, as reported in three communications by us, where we reported the finding of the EPR spectrum corresponding to FeIn in the trigonal configuration,[9] and the detection of a second orthorhombic spectrum which, in fact, was shown to be the spectrum corresponding to the ground state.[10,11] The aim of this paper is to present a complete analysis, including the hyperfine structure, of the orthorhombic EPR spectra and to derive the electronic structure of the FeIn pairs.

II. EXPERIMENTAL DETAILS

The samples were prepared from a Czochralski-grown, indium-doped silicon crystal with a resistivity of 2 Ω cm. The crystal was oriented and pieces were cut ($2.5\times2.5\times10$ mm^3) with the long axis parallel to ⟨110⟩. After evaporating iron onto the surface of the crystals, a sample was placed in a closed quartz ampoule. In the case of isotope doping, the evaporated iron was replaced by a piece of iron enriched to 96% in ^{57}Fe placed next to the silicon crystal. The ampoules were then evacuated and filled with argon gas. The diffusion took place at 1200 °C for 2 h before the samples were rapidly quenched. The EPR measurements were either performed in a Bruker ESP 300 spectrometer together with a helium-flow cryostat from Air Products, or in a ZWG ERS 230 spec-

trometer equipped with a liquid-hydrogen bath cryostat and a special, triaxial goniometer to facilitate the exact orientation of the sample. The spectrometers work in the X band, and the measurements were performed at temperatures between 4 and 40 K. In both spectrometers the sample could be illuminated *in situ*.

III. EXPERIMENTAL RESULTS AND ANALYSIS

In all samples the two previously reported spectra, LW and Lu4, of the orthorhombic iron-indium pair were detected.[10] Furthermore, upon illumination the trigonal FeIn spectrum, Lu2, was observed.[9] In Ref. 9, the Lu2 spectrum was analyzed in the effective spin $S'=\frac{1}{2}$ formalism, and the effective g' values as well as the hyperfine parameters were determined. These values are here given in Table I.

Also, the orthorhombic spectra can be analyzed using the effective spin $S'=\frac{1}{2}$ model, but, as was shown in Ref. 10, these spectra correspond to transitions within the two Kramers doublets of a zero-field-split, spin-$\frac{3}{2}$ system. The appropriate spin Hamiltonian can be written as

$$H_{FS}=D[S_z^2-\tfrac{1}{3}S(S+1)]+E[S_x^2-S_y^2]$$
$$+\mu_B[g_xB_xS_x+g_yB_yS_y+g_zB_zS_z]\ , \qquad (1)$$

where $x,y\|\langle 110\rangle$ and $z\|\langle 100\rangle$ and all symbols have their usual meaning. The zero-field splitting $\Delta=2(D^2+3E^2)^{1/2}$ is much larger than the microwave photon energy used and, therefore, only transitions within the two Kramers doublets of the $S=\frac{3}{2}$ system can be detected. This is the reason the spectrum can be treated approximately as two independent spectra and analyzed each with the $S'=\frac{1}{2}$ formalism in the magnetic-field range available with the spectrometer magnet used. The connection between the two representations can be obtained from perturbation-theory solutions for the eigenvalues of Eq. (1), from which effective g' values can be calculated for both doublets. A simpler procedure is to expand the exact eigenvalues of Eq. (1), which exist if the magnetic field is parallel to one of the three principal axes,[12] to second order in the ratio of Zeeman interaction to the zero-field splitting between the doublets. In this approach the values of the effective g' values ($S'=\frac{1}{2}$ formalism) are functions only of the real g values ($S=\frac{3}{2}$ formalism) and the ratio between the two fine-structure parameters E and D. This procedure was used in Ref. 10 to determine the real g values and the ratio E/D in the standard axis system.[13] If the assumption that $g\mu_BB\ll\Delta$ is insufficiently fulfilled for this approach, then higher-order contributions to the effective g' values must be taken into account. Since these contributions contain terms with a magnetic-field dependence, the effective g' values obtained vary with the microwave frequency. In the present case the $S'=\frac{1}{2}$ formalism is a good approximation for the observed transitions if the magnetic-field directions in the vicinity of the y axis are excluded. The breakdown of the approach using effective g' values for $B\|y$ is connected with the additional degeneracy between the states of the lower (if $D<0$) or upper (if $D>0$) doublet which occurs for any given value of E/D ($0\le E/D\le\frac{1}{3}$) when B is along the y axis at

$$g_y\mu_BB_d=2D[2E/D+2(E/D)^2]^{1/2}\ .$$

Clearly, if $h\nu<\Delta E_{12\max}$ (the maximum splitting $|E_1-E_2|$ between the two states of the doublet) in the magnetic-field range $(0,B_d)$, three lines may occur for $B\|y$. When B is rotated away from the y axis, the two high-field lines will move toward each other and disappear at a certain angle (looping transitions) which is dependent on the magnitude of the microwave photon energy. With the effective g' value approach, only the line at the lowest field is described. In the present case, $h\nu>\Delta E_{12\max}$, as can be seen in Fig. 1, and therefore only the line at the highest field can occur for $B\|y$. With the magnetic field in the vicinity of the y direction, the two lower lines turn into the high-field line in a very small angular region. The complete angular dependence of the EPR transitions is plotted in Fig. 2. The crosses represent experimental points and the solid lines the calculated rotation pattern using the real spin $S=\frac{3}{2}$, together with Eq. (1) and the parameters summarized in Table II. However, the value and sign of the parameter D were deduced from the temperature dependence of the intensities of the two transitions corresponding to LW and Lu4 and using the determined ratio E/D.[10,11] A determination of the fine-structure parameters from line positions was not possible because of the very weak dependence in the experimental region being used.

The EPR spectrum of the orthorhombic FeIn pair shows a rather complicated hyperfine structure (see Figs. 3–5). However, in the x direction the LW spectrum, which represents transitions within the upper doublet, shows a clear hyperfine splitting into ten lines, proving the existence of one indium ion in the defect.[10] Natural indium consists of two isotopes, 4.3% ^{113}In and 95.7% ^{115}In, which both have a nuclear spin $I=\frac{9}{2}$. Provided that there are only allowed hyperfine transitions, the hyperfine structure will consist of two sets of ten lines. However, since the nuclear gyromagnetic ratio is almost the same for the two isotopes and since the natural abundance is much larger for ^{115}In, only one set of ten lines can be detected. Isotope doping with ^{57}Fe ($I=\frac{1}{2}$) gave a further twofold splitting of the EPR lines (see Fig. 3 in Ref. 10) and it was thereby proved that the defect responsible for the spectrum consists of one In and one Fe atom. However, a detailed investigation shows a more compli-

TABLE I. Spin-Hamiltonian parameters for the trigonal ^{57}Fe^{115}In pair. The spectrum is analyzed within the effective spin $S'=\frac{1}{2}$ formalism.

$g'_\parallel=6.38\pm0.01$	$\lvert A'^{\,\mathrm{In}}_\parallel\rvert=(37\pm1)\times10^{-4}$ cm^{-1}	$\lvert A'^{\,\mathrm{Fe}}_\parallel\rvert=(1.2\pm0.3)\times10^{-4}$ cm^{-1}
$g'_\perp=1.08\pm0.01$	$\lvert A'^{\,\mathrm{In}}_\perp\rvert\le3\times10^{-4}$ cm^{-1}	$\lvert A'^{\,\mathrm{Fe}}_\perp\rvert=(3\pm1)\times10^{-4}$ cm^{-1}

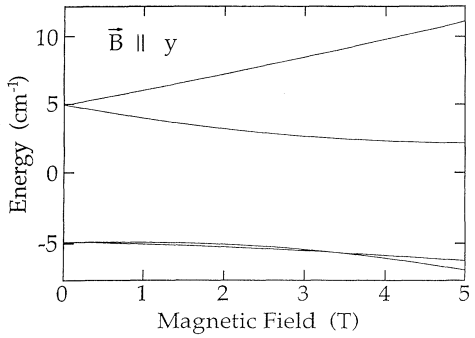

FIG. 1. Energy-level positions as a function of the magnetic field for a spin-$\frac{3}{2}$ system and the parameters given in Table II. The magnetic field is applied in the y direction.

cated structure, also in the x direction. Four of the ten lines are twofold split and there are also several additional lines with lower intensity, as shown in Fig. 3. An even more complex hyperfine structure is observed for the other principal directions, for intermediate directions of the magnetic field as well as for transitions within the lower doublet, because of the simultaneous appearance of allowed and forbidden hyperfine transitions. In order to describe the hyperfine structure the spin Hamiltonian [Eq. (1)] must be complemented by

$$H = H_{HF}^{\mathrm{In}} + H_Q^{\mathrm{In}} + H_{HF}^{\mathrm{Fe}} , \tag{2}$$

$$H_{HF}^{\mathrm{In}} = A_x S_x I_x + A_y S_y I_y + A_z S_z I_z - g_N \mu_N [B_x I_x + B_y I_y + B_z I_z] , \tag{3}$$

$$H_Q^{\mathrm{In}} = P_{\parallel} \{ [I_z^2 - \tfrac{1}{3} I(I+1)] + \tfrac{1}{3} \eta [I_x^2 - I_y^2] \} , \tag{4}$$

$$H_{HF}^{\mathrm{Fe}} = A_x S_x I_x + A_y S_y I_y + A_z S_z I_z , \tag{5}$$

where Eq. (3) represents the hyperfine and nuclear Zeeman and Eq. (4) the quadrupole interactions with the indium isotopes. Equation (5) is important only when doping is done with iron enriched in ^{57}Fe ($I = \frac{1}{2}$), since natural iron comprises 97.8% of isotopes with $I = 0$. The terms, reflecting the iron nuclear Zeeman interaction are omitted because its influence is estimated to be very small and not measurable. The principal axes of the hyperfine and quadrupole interaction tensors were assumed to coincide with those of **g** and **D**. In order to describe the hyperfine interaction, the total spin Hamiltonian, which is defined by Eqs. (1) and (2), was numerically diagonalized and, thus, the energy eigenvalues and eigenfunctions were found. From this it is possible to simulate the EPR spectrum and fit the spin-Hamiltonian parameters to the experimental one. In Figs. 3 and 4 such a comparison of

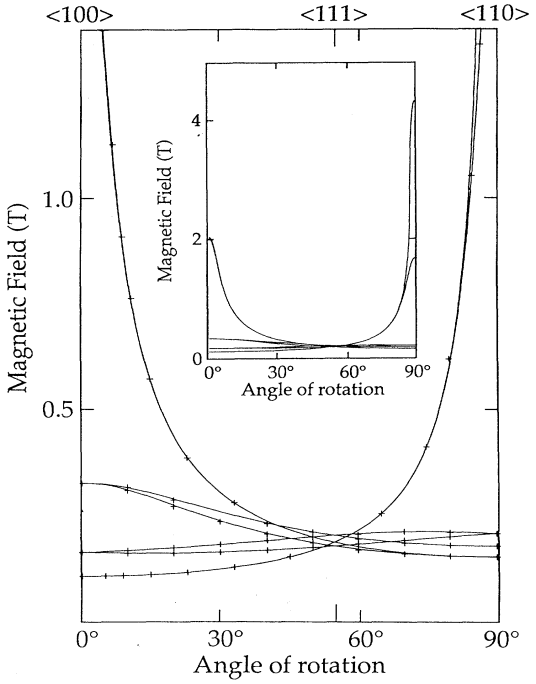

FIG. 2. The part of the calculated (using the $S = \frac{3}{2}$ model) angle-dependent resonance pattern which could be experimentally measured (up to 1.4 T). The experimental points are included. In the inset, the complete pattern is shown.

the hyperfine structure is shown for $B \| x$ and $B \| y$ for the transitions within the upper Kramers doublet (the LW spectrum). The close similarity between the experimentally determined and the calculated spectra is striking. The parameters determined in this way are given in Table II. Because of the complicated structure and the bad signal-to-noise ratio, it was not possible to determine the A_z (Fe) value within the limits of this work.

The additional structures observed in the experimental spectra are caused by the interaction with the neighboring ^{29}Si ions ($I = \frac{1}{2}$, 4.7%) in the different shells. This was not considered in the simulated spectra, because the resolution of the EPR spectra is too poor to make a reasonable fit of the silicon hyperfine constants of the different shells.

According to our analysis, the Lu4 and LW spectra correspond to transitions within the lower and upper doublets of a $S = \frac{3}{2}$ state with a large zero-field splitting. Therefore, in the $S = \frac{3}{2}$ formalism the hyperfine structure of the Lu4 spectrum should be described by the same spin Hamiltonian as the LW spectrum. In Fig. 5 the experimental Lu4 spectrum (top) with B in the z direction is

TABLE II. Spin-Hamiltonian parameters for the orthorhombic ^{57}Fe^{115}In pair. The spectrum is analyzed using Eq. (1) and $S = \frac{3}{2}$.

$D = (-4.9 \pm 1.0)$ cm^{-1}	$A_x^{\mathrm{In}} = (13.6 \pm 0.1) \times 10^{-4}$ cm^{-1}	$P_{\parallel}^{\mathrm{In}} = (-0.54 \pm 0.02) \times 10^{-4}$ cm^{-1}
$E/D = 0.052 \pm 0.006$	$A_y^{\mathrm{In}} = (-3.0 \pm 0.1) \times 10^{-4}$ cm^{-1}	$\eta^{\mathrm{In}} = -5.5 \pm 0.2$
$g_x = 2.07 \pm 0.02$	$A_z^{\mathrm{In}} = (-6.3 \pm 0.1) \times 10^{-4}$ cm^{-1}	$g_N^{\mathrm{In}} = 1.12 \pm 0.05$
$g_y = 2.05 \pm 0.02$	$\lvert A_x^{\mathrm{Fe}} \rvert = (5.2 \pm 0.2) \times 10^{-4}$ cm^{-1}	
$g_z = 2.09 \pm 0.01$	$\lvert A_y^{\mathrm{Fe}} \rvert = (7.5 \pm 1.0) \times 10^{-4}$ cm^{-1}	

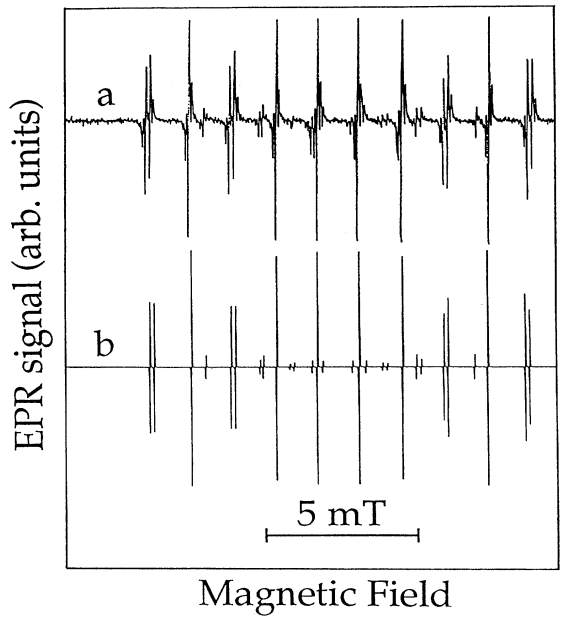

FIG. 3. (a) Experimental and (b) simulated hyperfine structure of the spectrum arising from the upper doublet (LW spectrum) with the magnetic field in the x direction.

shown together with the calculated one (bottom) *using exactly the same parameters as for the LW spectrum.* This fact and the similarity between the experimental and calculated spectra are independent and additional proof that the two spectra originate from the same defect.

Qualitatively, the complex hyperfine structure can be explained in the following way: The eigenstates of the Zeeman and fine-structure interactions given by $H(1)$ [the Hamiltonian in Eq. (1)] for the electronic transition considered here are denoted $|\psi_i\rangle$ (initial state) and $|\psi_f\rangle$ (final state). Since in the present case the splitting caused by the hyperfine and quadrupole interactions described

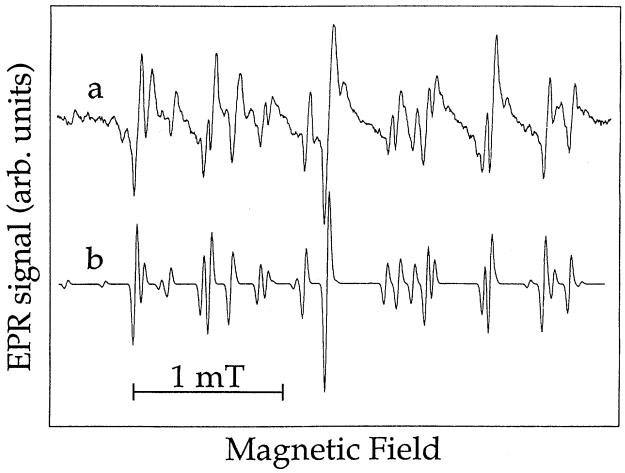

FIG. 4. (a) Experimental and (b) simulated hyperfine structure of the upper doublet (LW spectrum) with the magnetic field in the y direction.

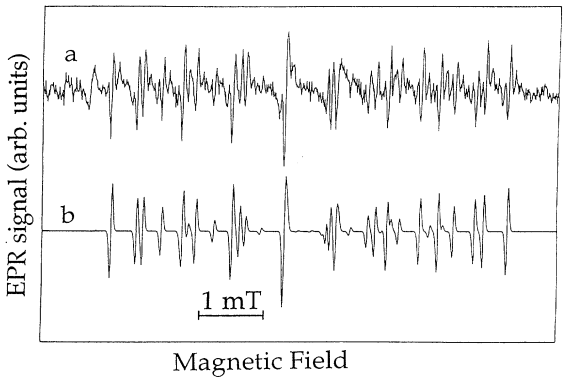

FIG. 5. (a) Experimental and (b) simulated hyperfine structure of the lower doublet (Lu4 spectrum) with the magnetic field in the z direction.

by Eq. (2) is small compared to that given by the electronic Zeeman and fine-structure terms $[H(2) \ll H(1)]$, the electronic parts of the eigenvalues of $H(2)$ are to a good approximation given by $\langle \psi_k | H(2) | \psi_k \rangle$, with $k = i,f$. In this approximation the whole hyperfine spin Hamiltonian $H(2)$ is diagonal in the electronic spin states. The indium hyperfine interaction described by Eq. (3) can be exactly diagonalized in the indium nuclear spin states by a suitable transformation of the indium nuclear axes. These interactions cause a splitting of both electronic states into ten equidistant levels, each of which we will label $|\psi_i, m\rangle$ and $|\psi_f, m'\rangle$, respectively. Here the indium nuclear quantum numbers m and m', which can take the values $-\frac{9}{2}, -\frac{7}{2}, \ldots, +\frac{9}{2}$, refer to the quantization axes $z'(i)$ and $z'(f)$ of the nuclear spin I in the electronic states $|\psi_i\rangle$ and $|\psi_f\rangle$. The relative transition probability for a nuclear transition $m \leftrightarrow m'$ during an electronic spin transition $\psi_i \leftrightarrow \psi_f$ is given by $|d_{mm'}(\delta)|^2$, where $d_{mm'}(\delta)$ are the real elements of the irreducible representation of the rotation group and δ denotes the angle between the nuclear quantization axes in the two electronic states $|\psi_i\rangle$ and $|\psi_f\rangle$.[14] With the magnetic field parallel to one of the principal axes (x,y,z), the angle δ amounts to 180° and, therefore, only the $2I+1$ allowed hyperfine lines with $m = m'$ appear. However, for intermediate directions of the magnetic field $\delta \neq 180°$, i.e., the $(2I+1)^2$ "allowed" and "forbidden" hyperfine transitions can occur. Including the quadrupole interaction described by Eq. (4), the quantization axes of the nuclear spin in both electronic states are changed, with the result that $\delta \neq 180°$ for all directions of the magnetic field and, therefore, forbidden hyperfine transitions will occur also for $B \| (x,y,z)$. The changes of the axes $z'(i)$ and $z'(f)$ and therefore the changes of the magnitude of δ are determined by the relation between the magnitude of the components of the hyperfine and quadrupole tensors and the nuclear Zeeman term. Also, the surprising symmetric splitting of four of the ten hyperfine lines for the upper doublet with $B \| x$ thus finds a simple explanation. In this case the quadrupole interaction causes only a very small deviation of the nuclear spin quantization axes from the quantization directions of the effective electronic spin parallel (final state) or antiparal-

lel (initial state) to the x axis, because the quadrupole interaction is strongest in this direction. The spectrum is therefore essentially determined by the allowed transitions $m-m'=0$ and only a few weak, forbidden transitions appear. This behavior is evident from the calculated energy levels, which are shown in Fig. 6. The equidistant splitting of the ten hyperfine levels in both electronic states described by $|x_i,m\rangle$ and $|x_f,m'\rangle$ is changed by the quadrupole interaction. The diagonal terms of the quadrupole interaction with respect to the quantization axis shift the energy levels but not, in the approximation considered, the transitions, since the levels are displaced equally proportional to m^2 in both electronic states and the selection rule for the hyperfine transitions $m-m'=0$ is unchanged. However, apart from a small shift of the energy levels, the off-diagonal elements of the quadrupole tensor cause a mixing of the states $|x_i,m\rangle$ with $|x_i,m\pm2\rangle$ and $|x_f,m'\rangle$ with $|x_f,m'\pm2\rangle$. Choosing the eigenfunctions $|\tilde{m}\rangle$ as linear combinations of $|m\rangle$ functions with m differing by 2, the 10×10 Hamilton matrix for each electronic state reduces to two 5×5 submatrices. The coupling coefficients are larger the smaller the energy distances between the states are. In our case the energy differences between the $|x_i+\frac{9}{2}\rangle$, $|x_i,+\frac{7}{2}\rangle$, and $|x_i,+\frac{5}{2}\rangle$, as well as between the $|x_f,-\frac{9}{2}\rangle$, $|x_f,-\frac{7}{2}\rangle$, and $|x_f,-\frac{5}{2}\rangle$, levels become very small. Therefore, the eigenfunctions $|x_i,+\frac{9}{2}\rangle$ and $|x_i,+\frac{5}{2}\rangle$ are essentially linear combinations of $|x_i+\frac{9}{2}\rangle$ and $|x_i,+\frac{5}{2}\rangle$. The mixing of the other states is comparatively small. Because the relative transition probability of the nuclear spin transitions is given by $|\langle\tilde{m}|\tilde{m}'\rangle|^2$, it is clear that there will be EPR transitions from $|x_i,+\frac{9}{2}\rangle$ and $|x_i,+\frac{5}{2}\rangle$ to $|x_f,+\frac{9}{2}\rangle$. Since the two levels $|x_i,+\frac{9}{2}\rangle$ and $|x_i,+\frac{5}{2}\rangle$ have almost the same energy, the two transitions will take place at almost the same magnetic field. In other words, the $|x_i,+\frac{9}{2}\rangle$ to $|x_f,+\frac{9}{2}\rangle$ transition seems to be split into two EPR lines. The next "split" is given by the corresponding transitions from the same initial levels to the $|x_f,+\frac{3}{2}\rangle$. In a similar way the two other "split" lines are the corresponding transitions caused by the strong mixing of the $|x_f,-\frac{9}{2}\rangle$ and $|x_f,-\frac{5}{2}\rangle$ levels.

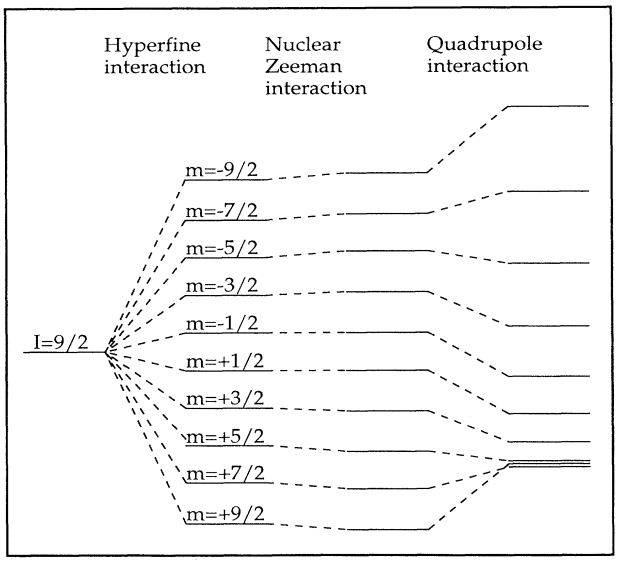

FIG. 6. Energy scheme of the nuclear levels for the initial electronic state of the upper doublet (LW spectrum) with the magnetic field in the x direction. The levels are labeled with their magnetic quantum numbers, taking the x axis as the quantization axis.

IV. DISCUSSION

In analogy with the other neutral iron-acceptor pairs, the neutral FeIn pairs can be well described by a substitutional, negatively charged acceptor with a closed shell and a positively charged iron ion at an interstitial position.[10,15] The electronic structure of such a pair is therefore expected to be identical to that of the Fe^+ state in a cubic field with a trigonal or orthorhombic distortion. In a cubic crystalline field the ^4F ground state of the $3d^7$ Fe^+ ion is split into two orbital triplets, $^4T_1$ and $^4T_2$, and an orbital singlet, $^4A_2$, with the $^4T_1$ state lowest in energy. This orbital triplet state is further split by the trigonal or rhombic fields caused by the acceptor ion. The schematic energy-level diagrams for the trigonal and orthorhombic defects are shown in Fig. 7. In accordance with the experimental results, the splitting behavior is given for a positive sign of the axial crystal-field parameter δ_{ax} for both cases.

The calculation of the g values and the zero-field-splitting parameters D and E of the Fe^+ and other related pair centers in silicon is a complex task. Following an approach originally proposed by Abragam and Pryce,[16] this problem has been treated by several authors[17–19] by restricting the calculation to the 12 base states of $^4T_1$ using an effective orbital momentum $L'=1$ and including the orbital contributions of excited states to the $^4T_1$ ground state through effective Landé factors. Within the $(2L'+1)(2S+1)$ manifold, the effect of the axial and rhombic fields and the spin-orbit interaction can be written as

$$H=H_{CF}+H_{LS}\ , \tag{6}$$

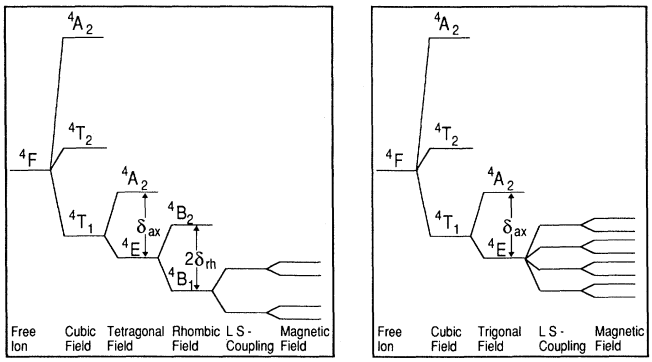

FIG. 7. Energy-level scheme for the $3d^7$ electronic configuration in a cubic crystal field with an orthorhombic (left) and a trigonal distortion (right).

TABLE III. Determined crystal field δ_{ax} and δ_{rh} and orbital Landé α parameters for the trigonal and orthorhombic iron-indium defect. Also shown are the calculated and experimentally determined effective g' values in the $S'=\frac{1}{2}$ approach and, for the orthorhombic defect, the energy distance Δ between the two lowest Kramers doublets.

					Calculated values				Experimental values		
Symmetry	δ_{ax} (cm^{-1})	δ_{rh} (cm^{-1})	α	Δ (cm^{-1})	g_x	g_y	g_z	Δ (cm^{-1})	g_x	g_y	g_z
Trigonal	+377	0	−0.325		1.08	1.08	6.38		1.08	1.08	6.38
Orthorhombic	+1831	95	−0.30	11	0.45	0.42	6.26	10	0.36	0.35	6.26
					3.51	4.35	2.07		3.80	4.42	2.07

$$H_{CF}=\delta_{ax}(\tfrac{2}{3}-L_z'^2)+\delta_{rh}(L_x'^2-L_y'^2)\ , \tag{7}$$

$$H_{LS}=\lambda(\alpha_x L_x' S_x+\alpha_y L_y' S_y+\alpha_z L_z' S_z)\ , \tag{8}$$

where δ_{ax} is the axial and δ_{rh} is the rhombic crystal-field parameter, λ is the spin-orbit coupling constant, and α_i ($i=x,y,z$) are the effective Landé factors. In the case of trigonal symmetry, $\delta_{rh}=0$. In a completely cubic crystal field and without covalence effects, α amounts to $-\frac{3}{2}$ in the weak-field and to -1 in the strong-field limit.[20] It should be noted that in this approach the fourth-order contributions from the acceptor-induced crystal field are not taken into account and, therefore, if z denotes the main axis, there is no differentiation between the trigonal and the tetragonal case. The combined effect of spin-orbit interaction and the trigonal or orthorhombic crystal field splits the ground state into six Kramers doublets, and the EPR transitions take place within the lowest or two lowest ones. The applied magnetic field lifts the remaining degeneracy and the Zeeman interaction can be described by the Hamiltonian

$$H_Z=\mu_B[B_x(\alpha_x L_x'+2S_x)+B_y(\alpha_y L_y'+2S_y)+B_z(\alpha_z L_z'+2S_z)]\ . \tag{9}$$

By combining Eqs. (6) and (9), the total effect of the crystal field, spin-orbit coupling, and magnetic field can be calculated, and, further, by using the eigenvalues and eigenfunctions obtained, the effective g' values, as a function of δ_{ax}, δ_{rh} and α_i, can also be found. The method described implies that the 12×12 matrix within the $^4T_1$ state has to be diagonalized. To simplify, we restricted the calculation to a single effective orbital Landé factor $\alpha=\alpha_x=\alpha_y=\alpha_z$ and used for the spin-orbit coupling constant $\lambda=-115\ cm^{-1}$, i.e., the value of the free Fe^+ ion, neglecting the reduction of its magnitude when the ion is incorporated in a semiconductor crystal.

For the trigonal defect $\delta_{rh}=0$, and, hence, only two parameters have to be fitted to the experimentally determined g' values: $g_\parallel'=6.38$ and $g_\perp'=1.08$. However, in order to attain these values, the orbital Landé factor had to be reduced to $\alpha\approx-0.3$. This is in analogy with the result from similar calculations on the trigonal FeB, FeAl, and FeGa pairs.[2] The EPR spectrum of isolated interstitial Fe^+ can be predicted in this model by letting $\delta_{ax}=0$, and also in this case it is necessary to use the value $\alpha\approx-0.3$ in order to get agreement between the calculated and experimentally determined g' values. This strong reduction of α was discussed by Ammerlaan and Gregorkiewicz, and covalent delocalization of the d electrons over silicon atoms in the vicinity of the impurity ion is assumed to be the predominant cause of this effect.[19] The result for the trigonal FeIn pair is shown in Table III.

In the case of the orthorhombic pair, it was possible to find fits with comparable agreement with the experimental data for different values of α. In this case we made the assumption that $\alpha=-0.3$ in analogy with the trigonal pairs. Also the relation δ_{rh}/δ_{ax} should be equal to the relation $E/D=0.052$ in the spin Hamiltonian. It is therefore only one parameter, δ_{ax}, which has to be fitted. The parameters for the optimum fit and the calculated and experimentally determined effective g' values are included in Table III. The agreement between the theoretically predicted values and the experimentally determined ones is not as good as in the trigonal case. The reasons for this might be that the fourth-order contribution of the crystal-field distortion is neglected, the rough approximation to fit the experimental results with one orbital Landé factor α, as well as the fact that the admixture of excited states is not included in the calculation.

V. CONCLUSIONS

The iron-indium pair in silicon has been studied using electron paramagnetic resonance. The hyperfine structures of the two orthorhombic spectra are analyzed in detail and the proposal that the two spectra are caused by a spin-$\frac{3}{2}$ system is supported. Both the trigonal and orthorhombic spectra are found to originate in transitions within the Kramers doublets of the $^4T_1$ manifold of the crystal field split ^4F ground state of the Fe^+ ion. The crystal fields caused by the acceptor ion as well as the orbital Landé factor are determined.

ACKNOWLEDGMENTS

The authors would like to thank K. Irmscher and J. Kreissl for useful comments. This work was supported by the Swedish Natural Science Research Council and the Swedish Board for Industrial and Technical Development.

*Permanent address: Arbeitsgrupp EPR in Wissenschaftler Interationsprogramm, Rudower Chaussee 5, D/O-1199 Berlin, FRG.

[1]G. W. Ludwig and H. H. Woodbury, in *Solid State Physics,* edited by F. Seitz and D. Turnbull (Academic, New York, 1962), Vol. 13, p. 223.

[2]J. J. van Kooten, G. A. Weller, and C. A. J. Ammerlaan, Phys. Rev. B **30**, 4564 (1984).

[3]W. Gehlhoff, K. Irmscher, and J. Kreissl, in *Proceedings of the Second International Autumn Meeting (GADEST), Garzau, 1987,* edited by H. Richter [Institute of Physics of Semiconductors, Frankfurt (Oder), 1987], p. 262.

[4]L. C. Kimerling, J. L. Benton, and J. J. Rubin, in *Defects and Radiation Effects in Semiconductors,* Proceedings of the Conference on Defects and Radiation Effects in Semiconductors, edited by R. R. Hasiguti, IOP Conf. Proc. No. 59 (Institute of Physics and Physical Society, Bristol, 1981), p. 215.

[5]H. Feichtinger, J. Oswald, R. Czaputa, P. Vogl, and K. Wünstel, in *Proceedings of the Thirteenth International Conference on Defects in Semiconductors,* edited by L. C. Kimerling and J. M. Parsey, Jr. (The Metallurgical Society of AIME, Warrendale, PA, 1985), p. 855.

[6]A. Chantre and D. Bois, Phys. Rev. B **31**, 7979 (1985).

[7]A. Chantre and L. C. Kimerling, in *Defects in Semiconductors,* Materials Science Forum Vols. 10–12, edited by H. J. von Bardeleben (Trans Tech Publications, Aedermannsdorf, Switzerland, 1986), p. 387.

[8]W. Gehlhoff, K. Irmscher, and U. Rehse, in *Defects in Semiconductors,* Materials Science Forum Vols. 38–41, edited by G. Ferenczi (Trans Tech Publications, Aedermannsdorf, Switzerland, 1989), p. 373.

[9]P. Omling, P. Emanuelsson, W. Gehlhoff, and H. G. Grimmeiss, Solid State Commun. **70**, 807 (1989).

[10]W. Gehlhoff, P. Emanuelsson, P. Omling, and H. G. Grimmeiss, Phys. Rev. B **41**, 8560 (1990).

[11]P. Emanuelsson, W. Gehlhoff, P. Omling, and H. G. Grimmeiss, in *Impurities, Defects and Diffusion in Semiconductors: Bulk and Layered Structures,* edited by Donald J. Wolford, Jerzy Bernholc, and Eugene Haller, MRS Symposia Proceedings No. 163 (Materials Research Society, Pittsburgh, 1990), p. 307.

[12]S. L. Hou, R. W. Summit, and R. Tucker, Phys. Rev. **154**, 258 (1967).

[13]C. Rudowicz and R. Bradley, J. Chem. Phys. **83**, 5192 (1985).

[14]W. Gehlhoff, Phys. Status Solidi B **88**, 599 (1978).

[15]P. Emanuelsson, P. Omling, H. G. Grimmeiss, W. Gehlhoff, J. Kreissl, K. Irmscher, and U. Rehse, in *Defects in Semiconductors 16,* Materials Science Forum Vols. 83–87, edited by G. Davies, G. G. DeLeo, and M. Stavola (Trans Tech Publications, Zürich, Switzerland, 1992), p. 137.

[16]A. Abragam and M. H. L. Pryce, Proc. R. Soc. London Ser. A **206**, 173 (1951).

[17]W. Gehlhoff and K. H. Segsa, Phys. Status Solidi B **115**, 443 (1983).

[18]C. A. J. Ammerlaan and J. J. van Kooten, in *Microscopic Identification of Electronic Defects in Semiconductors,* edited by Noble M. Johnson, Stephen G. Bishop, and George D. Watkins, MRS Symposia Proceedings No. 46 (Materials Research Society, Pittsburgh, 1985), p. 525.

[19]C. A. J. Ammerlaan and T. Gregorkiewicz, in *New Developments in Semiconductor Physics,* Lecture Notes in Physics Vol. 301 (Springer-Verlag, Berlin, 1988), p. 244.

[20]J. C. Griffith, *The Theory of Transition Metal Ions* (Cambridge University Press, Cambridge, England, 1961).